

Laboratory Studies of Potassium-Halide-Induced High-Temperature Corrosion of Superheater Steels. Part 1: Exposures in Dry Air

Hao Wu,* Patrik Yrjas, and Mikko Hupa

Laboratory of Inorganic Chemistry, Process Chemistry Centre, Åbo Akademi University, Piispankatu 8, FIN-20500 Turku, Finland

ABSTRACT: In recent years, some concerns about halogen (Cl, Br, and F)-related high-temperature corrosion in biomass- or waste-fired boilers have been raised. The presence of alkali chlorides in the deposits is believed to play a major role in high-temperature corrosion of the superheater steel materials in biomass- or waste-fired boilers. Available data are very scarce regarding alkali-bromide- or -fluoride-induced corrosion. This work has carried out using lab-scale high-temperature corrosion tests with three different superheater tube materials (10CrMo9-10, AISI 347, and Sanicro 28) exposed to KBr or KF at different temperatures (400–600 °C). At relatively low temperatures (≤ 550 °C), KBr and KF showed corrosivity similar to that of KCl. At 600 °C, KF showed much stronger corrosivity than either KBr or KCl, especially in the cases with the low-alloy steel 10CrMo9-10 and the austenitic steel AISI 347. At 550 °C and above, the oxide layers formed on the three steels were generally thicker and more uneven when exposed to KF compared to the results of the tests with KBr.

1. INTRODUCTION

High-temperature corrosion causes shutdowns, necessitates repairs of heat and power plants, and accounts for a significant fraction of total operating costs.^{1,2} Corrosion problems, which frequently occur on heat-transfer surfaces, such as superheaters and furnace water walls, increase with increasing temperatures and, thereby, limit the maximum steam temperature. Therefore, high-temperature corrosion of such areas constitutes one of the most important factors limiting the increase of thermal efficiency of steam boilers.³

In recent years, some concerns have been raised about halogen (Cl, Br, and F)-related high-temperature corrosion in biomass- and waste-fired boilers. Chlorine-related high-temperature corrosion has been studied extensively. The presence of alkali chlorides in the deposits is believed to play a major role in the corrosion observed in biomass- and waste-fired boilers.^{1–7}

Data related to high-temperature corrosion for bromine and fluorine are much less than that available for chlorine. Bromine is assumed to play a role similar to chlorine;^{8–14} the role of fluorine is even less understood. The main reason behind this lack of knowledge is the typically low Br and F concentrations in biomass or municipal solid waste (MSW). The sources of Br and F related to biomass or waste fuels are briefly reviewed below.

1.1. Occurrence of Bromine. In some anthropogenic waste, bromine is mainly found in the substances containing brominated flame retardants (BFRs). These substances are commonly used in electric and electronic equipment, such as circuit boards and equipment casings for television and personal computer housings, in plastic heat insulation foams used in the building sector, and in textiles and fabrics used in sofas, chairs, upholstery, and furniture cushions.^{11,13} Research has indicated that bromine in BFRs is bound in an organic matrix that readily decomposes during combustion in a manner similar to that of chlorine in polyvinyl chloride (PVC) plastic.^{11,15} Research has also shown that several weight percentages of Br can be found in waste from electric and electronic equipment (WEEE). A typical Br concentration in

mixed MSW was indicated to be about 50–200 mg/kg; this value can increase if the waste fuels are rich in flame-retarded plastics and textiles.^{10,14,16} Bromine is also widely used as both a disinfectant and a biocide in both industrial (e.g., pulp and paper mills and cooling water systems) and residential (pool, spa, and household detergents) water treatment systems. Because of these applications, bromine inevitably ends up in the industrial and municipal sewage sludge in concentrations ranging up to approximately 100 mg/kg. Bromine is also used in brominated soil fumigants and pesticides in agriculture; up to several hundred milligrams per kilogram of Br can be found as residual bromide in contaminated biological plants.¹⁴

1.2. Occurrence of Fluorine. Fluorine is commonly used in fluoropolymers, a family of high-performance plastics that are chemically inert, non-wetting, very slippery, non-stick, highly fire-resistant, high-temperature-resistant, highly weather-resistant, and regarded as non-toxic. Because of these extraordinary properties, fluoropolymers are used in a great variety of applications, e.g., in cable coating, silicon chips, wiring for laptop computers, cell phones, coated cookware, athletic and extreme-weather clothing, food-handling implements, and medical equipment. In 2004, global consumption of fluoropolymers reached 133 000 tons.¹⁷ The increasing global trend of fluoropolymer use means that larger amounts of disposed products containing fluoropolymers will eventually end up in municipal waste incineration plants. Huber et al.¹⁷ reported an investigation of waste produced in Norway in 2006, which indicated that paper (including coated paper and cardboard), plastic, and textiles are the main waste types containing fluoropolymers and other fluorinated organic compounds. In addition, fluorides, e.g., sodium fluoride (NaF), are often added to drinking water supplies and dental products, such as toothpastes and mouth rinses, to prevent dental cavities;¹⁸

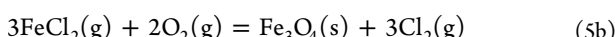
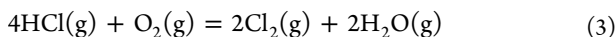
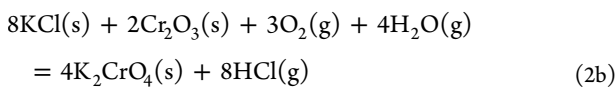
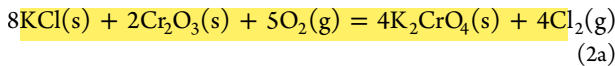
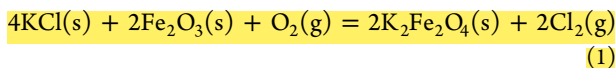
Received: October 7, 2014

Revised: January 8, 2015

Published: January 23, 2015

these fluorides may also end up in MSW and sewage sludge. A few studies^{8,16,19} have found several hundred milligrams per kilogram of F in MSW; however, this level could be much higher in some cases.

1.3. Alkali-Chloride-Induced Corrosion. Although the exact mechanisms behind chlorine- or alkali-chloride-induced corrosion are still controversial, a common hypothesis in the literature is a mechanism called “active oxidation”, during which a chlorine cycle is assumed to be involved. In active oxidation, chlorine is formed from a reaction between the condensed alkali chlorides, e.g., KCl, and the oxide scale on the metal, from which alkali ferrates and chromates are also produced (eqs 1 and 2a).²⁰ In the presence of water vapor, eq 2b is thought to take place.²¹ The chlorine gas, which is formed either from eqs 1 and 2a or via oxidation of HCl (g) (eq 3),^{20,22} can then penetrate the oxide layer to the scale/metal interface, where it reacts with the metal to form metal chlorides (eq 4). Because of the high vapor pressure of the metal chlorides, vaporization will take place. The volatile metal chlorides diffuse outward through cracks and pores of the scale to the scale/gas interface, where the metal chlorides are converted into metal oxides at a higher oxygen pressure (eqs 5a and 5b). The formed oxide scale has a highly porous structure and no protection against further corrosion. The chlorine released from eqs 5a and 5b can then penetrate the damaged oxide scale and react again according to eq 4.^{20,22–24}



1.4. Bromine- or Fluorine-Induced Corrosion. Literature is very scarce about the corrosion behavior of alloys in bromine- or fluorine-containing environments, such as HBr, Br₂, HF, F₂, and their derivative salts of metal halides. The possible corrosion effect of halogen in waste incinerators was raised by Rademakers et al.⁸ Their report mentioned that alloys containing elements that react with halogen gases (HCl, Cl₂, HBr, Br₂, HF, and F₂) to form low-melting and/or highly volatile metal halides can suffer severe high-temperature corrosion. Research has indicated that volatilization can be the dominant corrosion mechanism if the vapor pressure of a metal halide reaches or exceeds 10⁻⁴ atm.^{4,25} The melting temperatures of the most important metal halides (considering the major elements in alloys) and the temperatures at which their vapor pressure reaches 10⁻⁴ atm are shown in Table 1, which illustrates the minimal differences in the values of comparable bromides and chlorides. Analogous to the corresponding data shown for chlorides, the temperatures at which the vapor pressures reach 10⁻⁴ atm are much higher for nickel and chromium bromides than for iron bromides. Metal

Table 1. Melting Points of Fe, Cr, and Ni Chlorides, Bromides, and Fluorides and the Temperatures at Which Their Vapor Pressures Reach 10⁻⁴ atm²⁶

metal halide	melting point (°C)	temperature at 10 ⁻⁴ atm (°C)
FeCl ₂	676	536
FeCl ₃	303	167
CrCl ₂	820	741
CrCl ₃	1150	611
NiCl ₂	1030	607
FeBr ₂	689	509
FeBr ₃		156
CrBr ₂	842	716
CrBr ₃	>800	615
CrBr ₄		516
NiBr ₂	965	580
FeF ₂	1020	906
FeF ₃	1027	673
CrF ₂	894	928
CrF ₃	1404	855
NiF ₂	1450	939

fluorides require much higher temperatures than metal chlorides and bromides to reach a significant vapor pressure.

Combustion of halogen (Cl, Br, and F)-containing waste results in the formation of their hydride (HCl, HBr, and HF) gases as well as various organic halogen products.^{9,17} These hydride gases can combine with alkali metals (Na and K) to form alkali halides, which can deposit on the superheater tubes and waterwalls and probably enhance corrosion of these materials in a manner similar to alkali chlorides.

Vainikka et al.¹¹ performed a measurement campaign to determine the occurrence of corrosive ash-forming elements in a bubbling fluidized-bed (BFB) boiler co-firing solid recovered fuel (SRF) with spruce bark and paper mill wastewater sludge. Small amounts of alkali (K and Na) bromides combined with high concentrations of alkali chlorides were detected in the deposit sampled from the heavily corroded area at the bottom part of the back waterwalls. Iron oxide was also detected in the alkali-halide-rich area, demonstrating the contribution of halides in the corrosion process. In a similar test involving co-firing SRF and spruce bark and paper mill wastewater sludge in a BFB boiler as described by Vainikka et al.,¹³ bromine was found between the oxide scale and the membrane wall tube surface. Bromine was indicated to be in the form of PbBr₂, which would then react with iron in the steel in a manner similar to that of chlorine, forming FeBr₂. The research concluded that, in cases with a source of bromine in the fuel, corrosive high vapor pressure bromides can be formed in a manner analogous to that of chlorides.

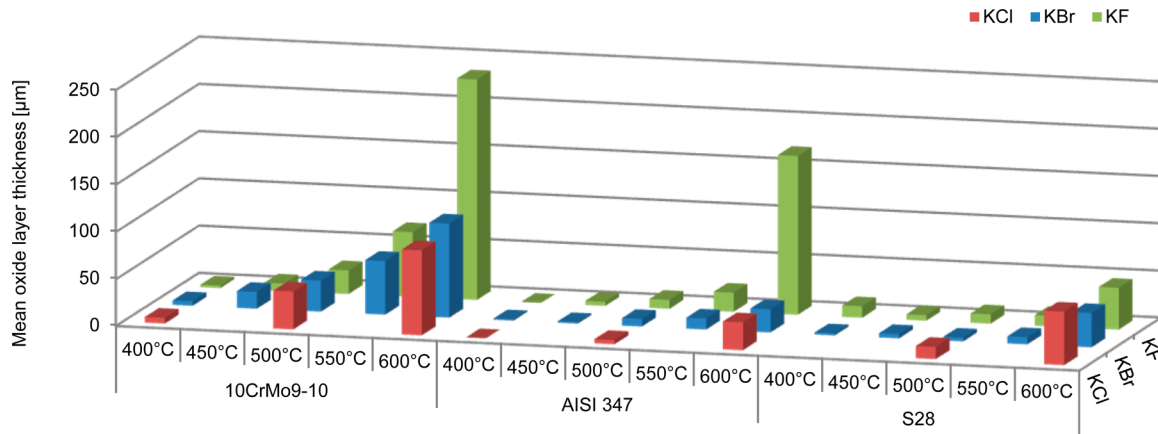
No experimental results are currently available on the high-temperature corrosion behavior of alloys exposed to alkali bromide or fluoride salt deposits. Therefore, this work has carried out lab-scale high-temperature corrosion tests of different superheater tube materials exposed to KBr or KF. The aim of this study was to obtain a better understanding of the role of KBr and KF in high-temperature corrosion of superheater steels.

2. MATERIALS AND METHODS

Three different superheater steel materials were used in the experiments: a low-alloy steel (10CrMo9-10), an austenitic stainless steel (AISI 347), and a high chromium and nickel austenitic stainless

Table 2. Elemental Compositions of the Tested Steels (wt %)

	Fe	Cr	Ni	Mo	Mn	Si	C	Nb	P	S
10CrMo9-10	95.96	2.24		1.00	0.45	0.25	0.07		0.01	0.01
AISI 347	68.74	18.08	10.92		0.92	0.46	0.04	0.81	0.02	0.01
Sanicro 28 (S28)	36.11	27.36	31.38	3.51	1.15	0.46	0.01		0.01	0.01

Figure 1. Mean oxide layer thicknesses at different temperatures of the steels exposed to KBr, KF, and KCl for 168 h in ambient air. KCl data are taken from Enestam et al.²³Table 3. Detailed Mean Oxide Layer Thicknesses (μm)^a

	10CrMo9-10					AISI 347				S28					
	400 °C	450 °C	500 °C	550 °C	600 °C	400 °C	450 °C	500 °C	550 °C	600 °C	400 °C	450 °C	500 °C	550 °C	600 °C
KCl	6	-	41	-	91	0	-	5	-	30	-	-	13	-	57
KBr	5	18	33	57	100	1	2	8	12	25	2	5	4	8	37
KF	3	8	25	69	233	0	4	10	21	168	12	6	10	11	45

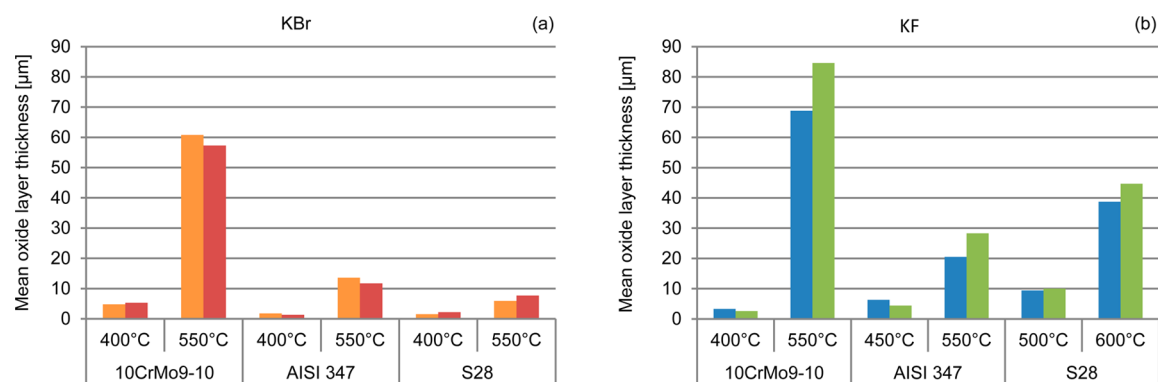
^a"-" indicates no test.

Figure 2. Reproducibility tests of 10CrMo9-10, AISI 347, and Sanicro 28 (S28) exposed to (a) KBr and (b) KF at different temperatures for 168 h.

steel (Sanicro 28). Table 2 presents the elemental compositions of the steels. The dimensions of the steel samples were 20 × 20 × 5 mm (length × width × thickness). Before the experiments, the steel samples were polished, washed, and then pre-oxidized for 24 h at 200 °C. After the pre-treatment, the steel samples were covered with 0.25 g of KBr or KF (2.5 g/cm³) with a particle size of 30–100 μm, placed in a horizontal tube furnace, and heat-treated at five different temperatures (400, 450, 500, 550, and 600 °C) in ambient air for 168 h (7 days). After the heat treatment, the samples were removed from the furnace, cooled to room temperature, and cast in resin as soon as possible. Each sample was then cut open in the middle to reveal the cross-section, which was then polished with kerosene before being studied by a scanning electron microscope (operated at 20 kV) equipped with an energy-dispersive X-ray detector (SEM/EDX).

The oxide layer thickness and the thickness distribution were measured at some 10 000 points over a 4 mm representative region of the cross-section using a panorama SEM technique, which has been well-described in detail in earlier publications.^{27–30} The corrosion attack was expressed as the mean thickness of the oxide layer. The elemental distributions in the oxide layer and steel and salt deposits were identified by X-ray images.

3. RESULTS AND DISCUSSION

3.1. Mean Oxide Layer Thickness. The mean oxide layer thickness values of all cases with KBr or KF are summarized in Figure 1 and Table 3. As those images show, corrosion occurred in most of the tests at temperatures well below the melting points of KBr (740 °C) and KF (857 °C). This

corresponds to observations regarding alkali-chloride-induced high-temperature corrosion in earlier publications.^{4,6,31} The results were also compared to tests with KCl from Enestam et al.²³ At relatively low temperatures (≤ 550 °C), KBr and KF showed corrosivity similar to KCl in the oxide layer thicknesses. At 600 °C, KF showed much stronger corrosivity than KBr and KCl, especially for the low-alloy steel, 10CrMo9-10, and for the austenitic steel, AISI 347.

The corrosion attack was generally more severe at higher temperatures. The iron-based steel, 10CrMo9-10, showed the highest degree of corrosion. The alloying elements, Cr and Ni, in austenitic steel clearly increased the corrosion resistance, as shown in the cases with AISI 347 and Sanicro 28. The higher content of Cr and Ni in Sanicro 28 than in AISI 347 did not necessarily improve the performance of Sanicro 28; in fact, Sanicro 28, in some cases, performed even worse than AISI 347, as strongly localized corrosion attack was observed.

3.2. Reproducibility. A number of parallel tests with each of KBr and KF were performed to check the reproducibility of the results. As shown in Figure 2, the results are generally highly reproducible.

3.3. SEM/EDX Analyses and Oxide Layer Thickness Distribution Curves.

3.3.1. Low-Alloy Steel, 10CrMo9-10. Testing resulted in noticeable corrosion attacks at a temperature as low as 400 °C on 10CrMo9-10 covered with KBr or KF. Figure 3 illustrates the thin and even oxide layer formed on

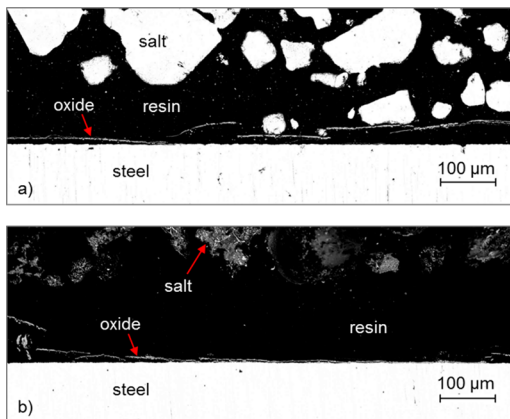


Figure 3. SEM images of 10CrMo9-10 exposed to (a) KBr and (b) KF at 400 °C for 168 h.

the steel. At 500 °C, the oxide layer became thicker with both KBr and KF, as shown in Figure 4. When the temperature was increased to 600 °C, 10CrMo9-10 suffered from extreme corrosion with both KBr and KF, with KF exhibiting a much stronger corrosivity than KBr (Figure 5).

Detachments between the oxide layer and the steel or within the oxide layer were visible in the SEM images for almost all tests. This likely occurred because of the thermal expansion differences between the oxide layer and the base steel or within the oxide layer itself during heating and cooling of the samples. In addition, the formation of highly volatile species, followed by evaporation and oxidation, may also lead to the layered oxide. The SEM images (Figures 3–5) illustrate that the amount of KF above the oxide layer seems to be significantly lower than that observed in the cases with KBr. This may, however, be an artifact of the experimental method because of the high hygroscopicity of KF. Even though the corroded sample was fixed in resin, KF on the surface of the cross-section of the cut

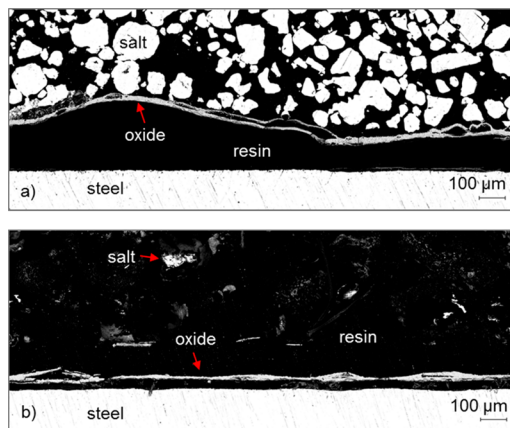


Figure 4. SEM images of 10CrMo9-10 exposed to (a) KBr and (b) KF at 500 °C for 168 h.

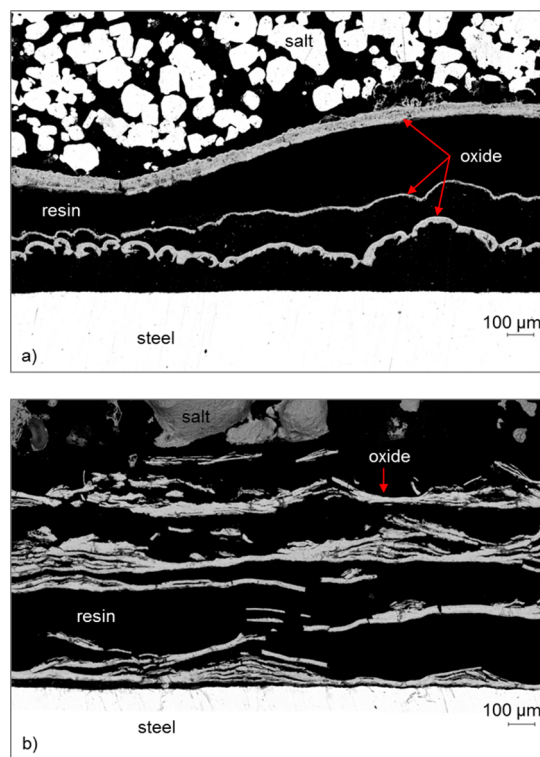


Figure 5. SEM images of 10CrMo9-10 exposed to (a) KBr and (b) KF at 600 °C for 168 h.

sample could absorb moisture from air and may have been partially removed during the polishing process.

With KBr, the oxide layer that was formed on 10CrMo9-10 generally looked quite compact despite the detachment, as shown in Figures 3–5. However, at 500 °C and above, locally occurring porous iron oxide areas (arrows 1 and 2 in Figure 6) were observed above the compact oxide layer (arrow 3). The salt particles in close proximity to this porous iron oxide seem to have been partially molten (Figure 6). This kind of porous iron oxide was first observed at 525 °C in a test with 10CrMo9-10 exposed to KCl by Enestam et al.,²³ who attributed the formation of the porous iron oxide to vaporization of metal chlorides and their subsequent oxidation and condensation. As shown earlier in Table 1, the volatile behaviors of FeBr₂ and FeCl₂ are quite similar. The vapor pressures of FeBr₂ and FeCl₂

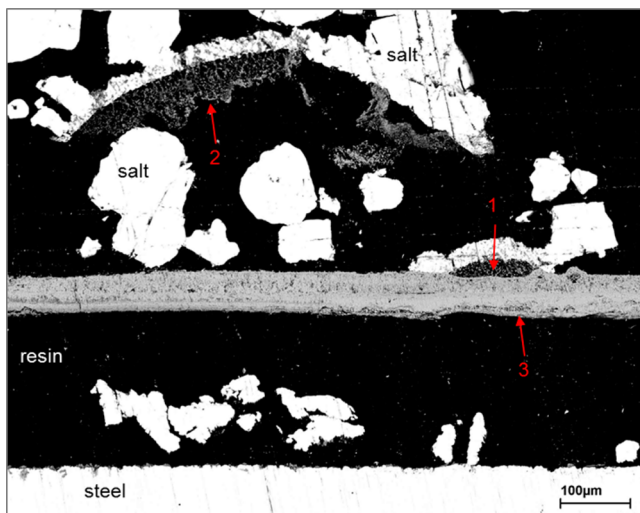


Figure 6. SEM image of 10CrMo9-10 exposed to KBr at 550 °C for 168 h, showing localized porous iron oxide formation.

reach 10^{-4} atm at about 500 °C. Therefore, it is reasonable to speculate that the porous iron oxide observed in our tests with KBr is attributable to the vaporization of iron bromide in a manner analogous to that of iron chloride, followed by subsequent oxidation and condensation.

This kind of porous iron oxide was, however, not observed with KF. This might be explained by the low volatility of FeF₂ at the test temperatures. According to Table 1, the temperature needs to be above 906 °C for the vapor pressure of FeF₂ to reach 10^{-4} atm.

The compact oxide layers formed on 10CrMo9-10 with KBr and KF mainly contained iron oxide and some small amounts of chromium oxide. Typically, the outer layer was rich in iron oxide, while the inner layer was rich in chromium oxide. An example of an X-ray map of 10CrMo9-10 with KBr at 550 °C is shown in Figure 7, which illustrates that the inner oxide layer close to the steel consisted of both iron and chromium oxide but the outer part of the oxide layer contained pure iron oxide and no chromium oxide at all.

The oxide layer thickness distribution curves over a 4 mm region of the cross-section from tests at different temperatures are shown in Figure 8. At 400 °C, the curves for both salts are very narrow, indicating a thin and even oxide layer formation. With an increasing temperature, the curves become wider and flatter. This is more pronounced for 10CrMo9-10 with KF than with KBr at 600 °C, which confirms the earlier observation from the SEM image that the oxide layer formed on 10CrMo9-10 with KF is much thicker and more uneven than with KBr.

3.3.2. Austenitic Stainless Steel, AISI 347. With both salts, KBr and KF, the austenitic stainless steel, AISI 347, showed better corrosion resistance than the low-alloy steel, 10CrMo9-10. At 400 and 450 °C, a very thin oxide layer (<5 μm) was formed on the steel with both KBr and KF. The oxide layer was

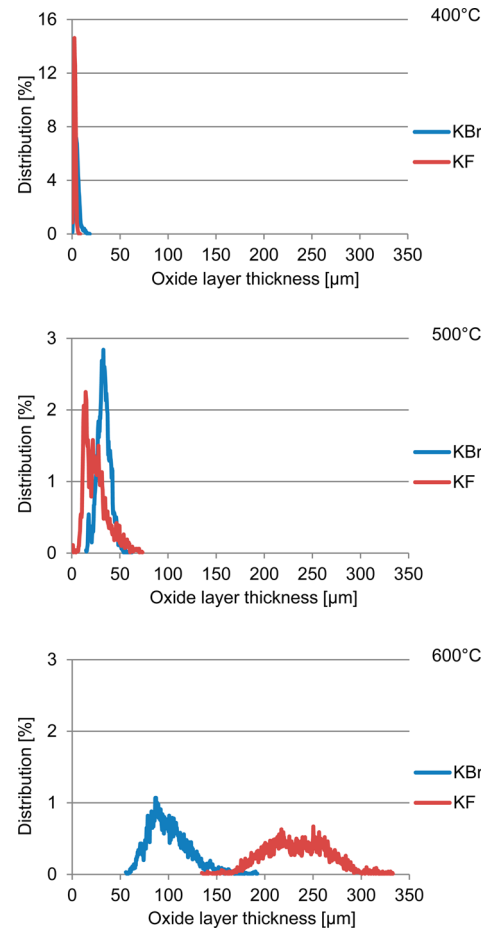


Figure 8. Oxide layer thickness distribution curves of 10CrMo9-10 exposed to KBr and KF for 168 h at 400, 500, and 600 °C.

not very uniform and, at some points, was undetectable. A clearly measurable oxide layer (~10 μm) began to form at 500 °C with each salt.

With KBr at 600 °C, a strongly localized corrosion attack with some grain boundary corrosion (i.e., cracks along the grains typically with angles of ~120°) and internal pitting was observed on AISI 347 (Figure 9). As seen from the X-ray maps in Figure 10, the pitting area contained mainly chromium oxide (arrow 4) and some nickel oxide (arrow 5). A metallic nickel-rich layer also remained on the basic steel surface (arrow 7). A compact oxide layer above the steel consisted of Fe–Cr–Ni oxide, where the upper part was rich in iron oxide (arrow 2), while the lower part contained mainly chromium oxide (arrow 3) together with some nickel oxide (arrow 6). A locally formed porous iron oxide was found on top of the compact oxide layer; it grew around and mixed with the salt particles. The salt particles mixed with this porous iron oxide appear to have been partially molten (arrow 1). This kind of porous iron oxide has been observed by Enestam et al.²³ in a test with AISI 347 and

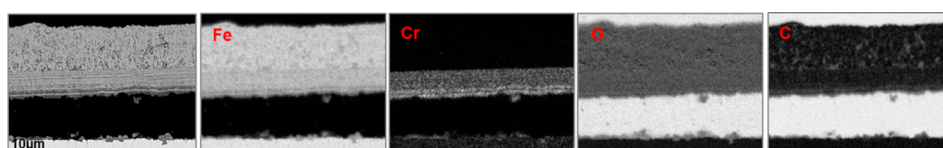


Figure 7. X-ray maps of 10CrMo9-10 exposed to KBr at 550 °C for 168 h.

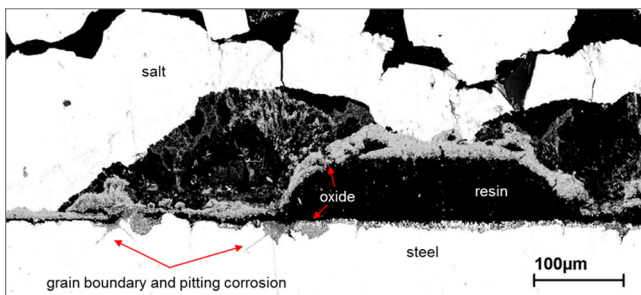


Figure 9. SEM image of AISI 347 exposed to KBr at 600 °C for 168 h, showing grain boundary and pitting corrosion.

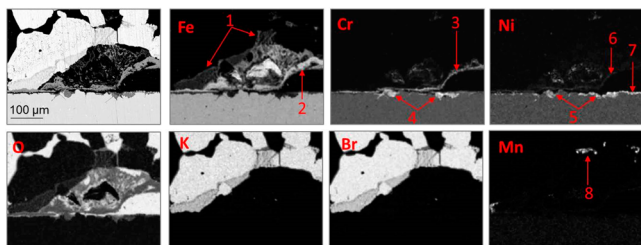


Figure 10. X-ray maps of AISI 347 exposed to KBr at 600 °C for 168 h.

KCl at 575 °C. Moreover, for AISI 347, a small amount of manganese oxide (arrow 8) was detected around the salt particles. This Mn oxide was probably formed by the evaporation of manganese bromide, followed by subsequent oxidation and condensation.

In addition, with KBr at 600 °C, a different kind of compact oxide (arrow 1) of a darker gray shade was formed locally just on top of the Fe–Cr–Ni compact oxide (arrow 2), between and around the salt particles, as shown in the SEM image in Figure 11a. The X-ray maps in Figure 12a show that the three elements K, Cr, and O were present in this area (arrow 1). The quantification spot analysis presented in Table 4 showed that

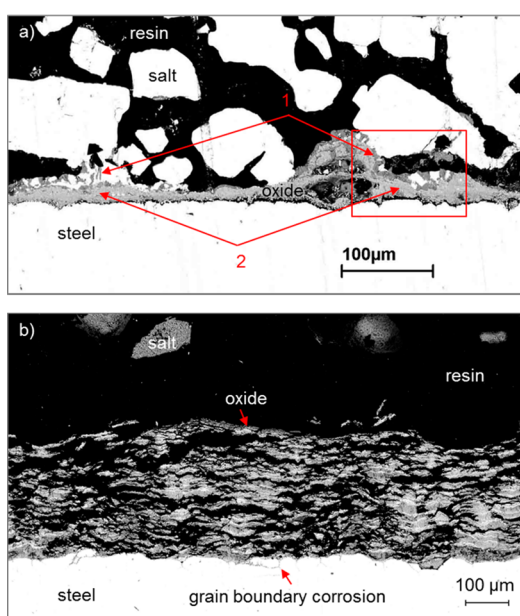


Figure 11. SEM images of AISI 347 exposed to (a) KBr and (b) KF at 600 °C for 168 h.

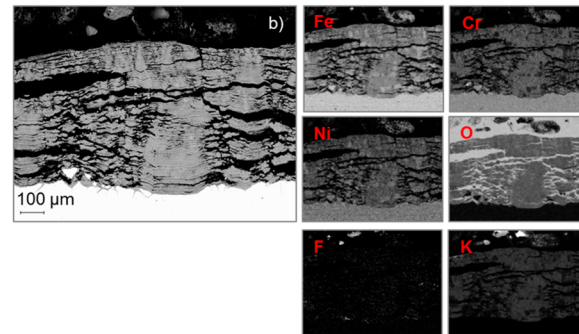
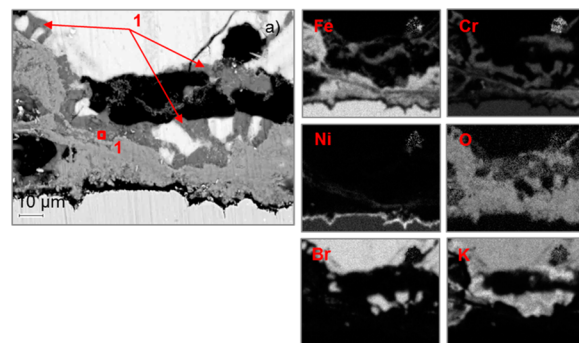


Figure 12. X-ray maps of AISI 347 exposed to (a) KBr and (b) KF at 600 °C for 168 h, with potassium chromate observed.

Table 4. Quantification Analysis of Spot 1

element	O	S	K	Cr	Fe	Ni	Br
spot 1 (atom %)	56.79	0.14	27.11	14.40	0.53	0.13	0.90

this area most likely consisted of K_2CrO_4 (potassium chromate), because the atomic ratio of K/Cr/O was about 2:1:4. The formation of K_2CrO_4 indicates a reaction between KBr and chromium oxide. The formation of potassium chromate was also observed in the test with AISI 347 and KBr at 500 °C but not at lower temperatures. Similar results were also observed by Enestam et al.²³ in a test with AISI 347 and KCl at 500 °C and by Lehmusto et al.²¹ in a test with 304L (a stainless steel similar to AISI 347) and KCl at 500 °C.

Furthermore, on the basis of Figure 11a, this K_2CrO_4 appears to have been partially molten together with KBr at 600 °C. This may be related to the findings of a study by Shinata,³¹ who reported the role of Na_2CrO_4 in accelerated oxidation of Cr induced by NaCl. Shinata proposed that Na_2CrO_4 decreased the melting point of NaCl by forming a NaCl– Na_2CrO_4 eutectic with a reported temperature of 577 °C. Once the eutectic mixture was formed, the oxidation reaction continued in the melt or through the melt, which prevented the formation of a protective scale. The same mechanism can be speculated to be valid for the test with KBr, in which a KBr– K_2CrO_4 eutectic was most likely formed and played a similar role in the accelerated oxidation. The eutectic temperature was reported to be 629 °C,³² which is close to the test temperature.

In the tests with KF, no melt was observed between the oxide scale and the salt particles. At 500 °C and above, a Fe–Cr–Ni oxide together with K but not with F was observed on AISI 347 (Figure 12b). However, confirming the exact K compound is difficult. K_2CrO_4 is the most likely compound, assuming that KF performed in a manner similar to KCl and KBr, initiating the “active oxidation” by destroying the protective Cr_2O_3 ,

Furthermore, that fact that F was not observed in the oxide scale implies that it exited in gaseous form.

In addition, much more metal (Fe, Cr, and Ni) oxidation occurred in the test with KF than with KBr at temperatures above 500 °C (e.g., panels a and b of Figure 12). However, it cannot simply be explained by the volatilization and outward diffusion of metal halide, followed by oxidation at the scale/gas interface, because the vapor pressures would indicate that the metal (Fe, Cr, and Ni) bromide is more volatile than the corresponding metal fluoride (Table 1). As shown in Figure 12b, a large amount of K (assumed as K_2CrO_4) embedded throughout the oxide layer in the test with KF at 600 °C, while in the case with KBr, K_2CrO_4 was formed locally just on top of the Fe–Cr–Ni compact oxide (Figure 12a). In the case with KF, the significant formation of K_2CrO_4 probably increased the porosity of the oxide layer and assisted the inward diffusion of O_2 , which can enhance the inward oxidation of metal fluorides close to the scale/metal interface. This may explain why significant metal (Fe, Cr, and Ni) oxidation occurred without the volatilization of metal fluorides at 600 °C.

In the tests with KF, grain boundary corrosion was observed at 550 °C and higher (Figure 11b). AISI 347 with KF clearly suffered from more severe corrosion at 600 °C compared to the tests at lower temperatures (≤ 550 °C).

Figure 13 shows the oxide layer thickness distribution curves for AISI 347 with KBr and KF at 500, 550, and 600 °C. The curves become wider and flatter with increasing temperature.

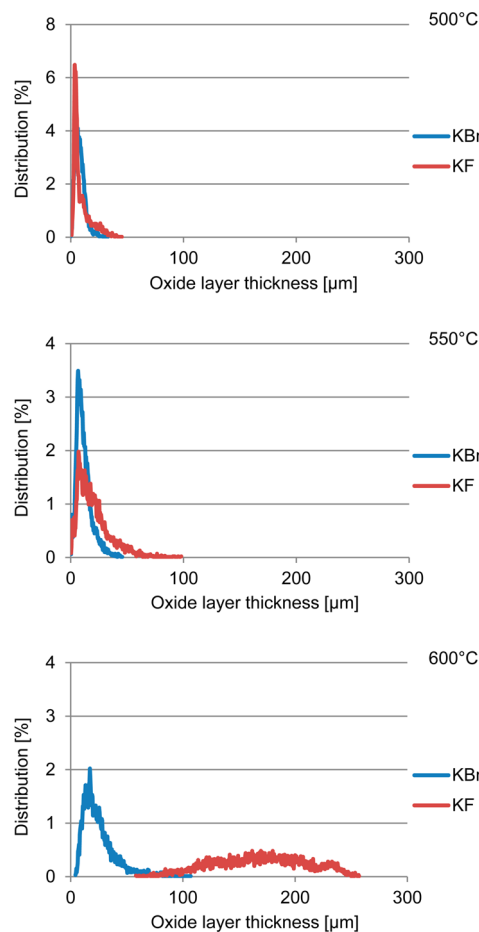


Figure 13. Oxide layer thickness distribution curves of AISI 347 exposed to KBr and KF for 168 h at 500, 550, and 600 °C.

This is more pronounced for AISI 347 with KF than with KBr at 550 and 600 °C, indicating that the oxide layer formed on AISI 347 with KF is much thicker and more uneven than that formed with KBr.

3.3.3. High Chromium and Nickel Austenitic Steel, Sanicro 28

The steel Sanicro 28, with its higher Cr and Ni content, started to corrode locally at 400 °C with each salt, with KF causing substantially higher local corrosion than KBr (panels a and b of Figure 14). With KBr at 400 °C, a Fe–Cr–Ni oxide

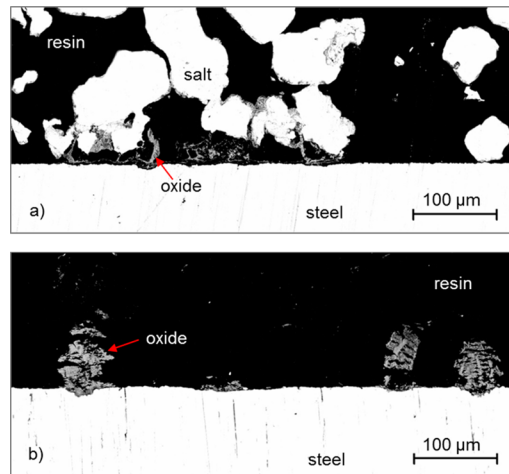


Figure 14. SEM images of Sanicro 28 exposed to (a) KBr and (b) KF at 400 °C for 168 h.

was formed locally on the steel surface and also around and between the salt particles. With KF at 400 °C, a Fe–Cr–Ni oxide was mainly formed locally on the steel surface.

In the tests with KBr and KF, K was observed in the oxide layer, most likely as K_2CrO_4 , at 450 °C and above (panels a and b of Figure 15), while with KCl, it became visible at 500 °C in the test by Enestam et al.²³ With KBr at 600 °C (Figure 15a), a

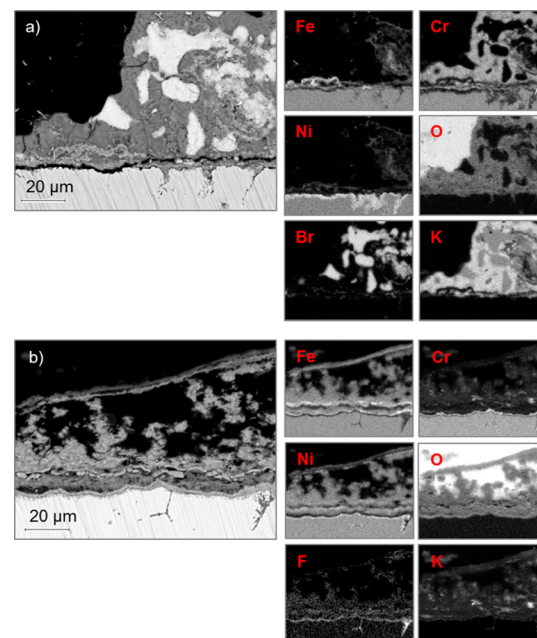


Figure 15. X-ray maps of Sanicro 28 exposed to (a) KBr and (b) KF at 600 °C for 168 h.

large amount of K_2CrO_4 was observed in the upper part of the oxide layer, growing around and between the salt particles. Similar to the condition observed for AISI 347 with KBr, this K_2CrO_4 formed on Sanicro 28 also appears to have been partially molten together with KBr, probably because of the formation of a KBr– K_2CrO_4 eutectic. The lower part of the oxide layer consisted of a Fe–Cr–Ni oxide, and the internally attacked area was rich in chromium oxide. Because of the depletion of Fe and Cr, a nickel-rich metallic layer remained on the steel surface.

In some tests with KF, F formed a continuous layer at the metal/oxide interface and along the grain boundaries. This fluoride was most likely either potassium fluoride or chromium fluoride, according to the X-ray maps in Figure 15b. In addition, Figure 15b shows that K (assumed as K_2CrO_4) was distributed throughout the oxide layer in the test with KF at 600 °C. Much more metal (Fe and Ni) oxide was formed in the upper part of the oxide layer in the test with KF (Figure 15a) than with KBr (Figure 15b) at 600 °C. The corrosion mechanism of Sanicro 28 with KF looks similar to that of AISI 347 with KF, as discussed in section 3.3.2. The significant formation of K_2CrO_4 probably increased the porosity of the oxide layer and assisted the inward diffusion of O_2 , which can enhance the inward oxidation of metal fluorides close to the scale/metal interface.

Some local grain boundary corosions became visible on Sanicro 28 at 550 and 600 °C with both KBr and KF (panels a and b of Figure 16). As observed for AISI 347, Sanicro 28 exposed to KF suffered from significant corrosion at 600 °C, to a greater extent than at the other test temperatures.

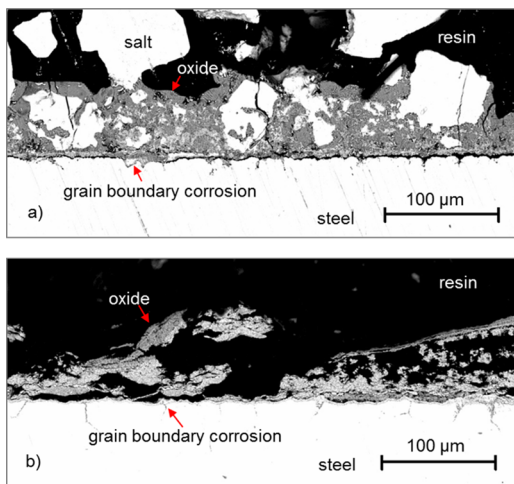


Figure 16. SEM images of Sanicro 28 exposed to (a) KBr and (b) KF at 600 °C for 168 h.

Figure 17 shows the oxide layer thickness distribution curves for Sanicro 28 exposed to KBr and KF at 500, 550, and 600 °C. As observed for 10CrMo9-10 and AISI 347, Sanicro 28 with KF also showed a wider and flatter distribution curve than with KBr at 550 and 600 °C, which confirms the higher corrosivity of KF than KBr at higher temperatures.

4. CONCLUSION

In this study, laboratory high-temperature corrosion tests with 10CrMo9-10, AISI 347, and Sanicro 28 exposed to KBr or KF at a fixed temperature (400–600 °C) in ambient air for 168 h (7 days) were carried out. The results were compared to an

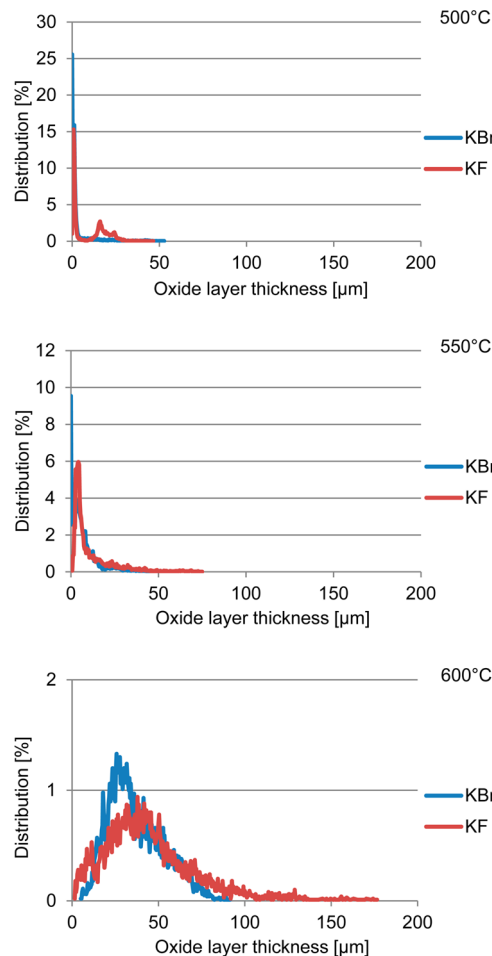


Figure 17. Oxide layer thickness distribution curves of Sanicro 28 exposed to KBr and KF for 168 h at 500, 550, and 600 °C.

earlier published paper, in which the same steels were exposed to KCl. The conclusions here include all three alkali halides for a more complete overview of their corrosion behaviors, although the work involving KCl was published earlier by Enestam et al.²³ The following conclusions can be made: (1) Corrosion occurred in most of the tests at temperatures well below the melting points of KBr (740 °C) and KF (857 °C). (2) The corrosion attack was generally more severe at higher temperatures. (3) At relatively low temperatures (≤ 550 °C), KBr and KF showed corrosivity similar to that of KCl when comparing the oxide layer thicknesses. At 600 °C, KF showed much stronger corrosivity than KBr and KCl, especially in the cases with the low-alloy steel, 10CrMo9-10, and the austenitic steel, AISI 347. (4) When 10CrMo9-10 and AISI 347 were exposed to KBr at 500 °C and above, a local porous iron oxide was observed on top of the compact oxide layer and also grew around and through the salt particles. The salt particles in close proximity to this porous iron oxide seem to have been partially molten. This kind of porous iron oxide may have been formed through the vaporization of iron bromide, followed by the subsequent oxidation and condensation. This kind of porous iron oxide was first observed with KCl at temperatures above 500 °C but not observed with KF at any of the test temperatures. (5) The austenitic steel, AISI 347, and the high chromium and nickel steel, Sanicro 28, showed better corrosion resistance to KBr, KF, and KCl than 10CrMo9-10; however, some local corrosion attack was observed on both AISI 347 and

Sanicro 28 at a temperature as low as 400 °C. (6) Potassium, most likely as potassium chromate (K_2CrO_4), was observed in the oxide layer for AISI 347 and Sanicro 28 with KBr, KF, and KCl at 500 °C and above. Furthermore, this K_2CrO_4 appears to have been partially molten together with KBr at 600 °C for both AISI 347 and Sanicro 28, probably because of the formation of a KBr– K_2CrO_4 eutectic. However, in the tests with KF, no melt was observed between the oxide scale and the salt particles. Contrary to the tests with KBr, the tests with KF at 600 °C caused significant formation of K_2CrO_4 embedded throughout the oxide layer on AISI 347 and Sanicro 28, which probably increased the porosity of the oxide layer and assisted the inward diffusion of O_2 , which can enhance the inward oxidation of metal fluorides close to the scale/metal interface. (7) Some local grain boundary corosions were observed for AISI 347 and Sanicro 28 with KBr, KF, and KCl at temperatures above 500 °C. (8) At 550 °C and above, the oxide layer formed on the three steels with KF was generally thicker and more uneven than that observed with KBr.

In general, KBr and KF were confirmed to be detrimentally corrosive to the superheater steel materials. When 10CrMo9-10 is exposed to KBr- or KF-containing deposits, the steel temperature is suggested to be lower than 500 °C to avoid enhanced corrosion. AISI 347 and Sanicro 28, having better corrosion resistance than 10CrMo9-10, could be durable up to 550 °C with KBr-containing deposits and up to only 500 °C with KF-containing deposits. In a waste incinerator with a high content of potassium halide deposits, high-temperature corrosion problems could be mitigated by either reducing operating temperature or reducing the potassium halide content in the deposit by co-combustion or use of sulfur/sulfate-containing additives. To keep the thermal efficiency of the boiler, the latter suggestion is usually adopted practically. All tests in this work were conducted in ambient air, and the influence of different gases (H_2O , SO_2 , CO_2 , etc.) should be studied in future work.

AUTHOR INFORMATION

Corresponding Author

*E-mail: hwu@abo.fi.

Notes

The authors declare no competing financial interest.

ACKNOWLEDGMENTS

This work has been carried out within FUSEC (2011–2014) as part of the activities of the Åbo Akademi Process Chemistry Centre. Other research partners are VTT, Lappeenranta University of Technology, Aalto University, and Tampere University of Technology. Support from the National Technology Agency of Finland (Tekes), Andritz Oy, Metso Power Oy, Foster Wheeler Energia Oy, UPM-Kymmene Oyj, Clyde Bergemann GmbH, International Paper, Inc., and Top Analytica Oy Ab is gratefully acknowledged.

REFERENCES

- (1) Broström, M.; Kassman, H.; Helgesson, A.; Berg, M.; Andersson, C.; Backman, R.; Nordin, A. Sulfation of corrosive alkali chlorides by ammonium sulfate in a biomass fired CFB boiler. *Fuel Process. Technol.* **2007**, *88*, 1171–1177.
- (2) Lee, S.; Themelis, N. J.; Castaldi, M. J. High-temperature corrosion in waste-to-energy boilers. *J. Therm. Spray Technol.* **2007**, *16*, 104–110.

(3) Persson, K.; Brostrom, M.; Carlsson, J.; Nordin, A.; Backman, R. High temperature corrosion in a 65 MW waste to energy plant. *Fuel Process. Technol.* **2007**, *88*, 1178–1182.

(4) Nielsen, H. P.; Frandsen, F. J.; Dam-Johansen, K.; Baxter, L. L. The implications of chlorine-associated corrosion on the operation of biomass-fired boilers. *Prog. Energy Combust. Sci.* **2000**, *26*, 283–298.

(5) Salmenoja, K.; Makela, K.; Hupa, M.; Backman, R. Superheater corrosion in environments containing potassium and chlorine. *J. Inst. Energy* **1996**, *69*, 155–162.

(6) Salmenoja, K. Field and laboratory studies on chlorine-induced superheater corrosion in boilers fired with biofuels. Ph.D. Thesis, Åbo Akademi University, Åbo Akademis Tryckeri, Åbo, Finland, 2000; Report 00-6.

(7) Hansen, L. A.; Nielsen, H. P.; Frandsen, F. J.; Dam-Johansen, K.; Hörlück, S.; Karlsson, A. Influence of deposit formation on corrosion at a straw-fired boiler. *Fuel Process. Technol.* **2000**, *64*, 189–209.

(8) Rademakers, P.; Hesseling, W.; van de Wetering, J. *Review on Corrosion in Waste Incinerators, and Possible Effect of Bromine*; TNO Industrial Technology: Apeldoorn, Netherlands, 2002; TNO Report I02/01333/RAD.

(9) Vehlow, J.; Bergfeldt, B.; Hunsinger, H.; Seifert, H.; Mark, F. E. Bromine in waste incineration: Partitioning and influence on metal volatilization. *Environ. Sci. Pollut. Res. Int.* **2003**, *10*, 329–334.

(10) Vehlow, J.; Mark, F. E. Influence of bromine on metal volatilization in waste combustion. *J. Mater. Cycles Waste Manage.* **2000**, *2*, 89–99.

(11) Vainikka, P.; Bankiewicz, D.; Frantsi, A.; Silvennoinen, J.; Hannula, J.; Yrjas, P.; Hupa, M. High temperature corrosion of boiler waterwalls induced by chlorides and bromides. Part 1: Occurrence of the corrosive ash forming elements in a fluidised bed boiler co-firing solid recovered fuel. *Fuel* **2011**, *90*, 2055–2063.

(12) Bankiewicz, D.; Vainikka, P.; Lindberg, D.; Frantsi, A.; Silvennoinen, J.; Yrjas, P.; Hupa, M. High temperature corrosion of boiler waterwalls induced by chlorides and bromides—Part 2: Lab-scale corrosion tests and thermodynamic equilibrium modeling of ash and gaseous species. *Fuel* **2012**, *94*, 240–250.

(13) Vainikka, P.; Enestam, S.; Silvennoinen, J.; Taipale, R.; Yrjas, P.; Frantsi, A.; Hannula, J.; Hupa, M. Bromine as an ash forming element in a fluidised bed boiler combusting solid recovered fuel. *Fuel* **2011**, *90*, 1101–1112.

(14) Vainikka, P.; Hupa, M. Review on bromine in solid fuels—Part 2: Anthropogenic occurrence. *Fuel* **2012**, *94*, 34–51.

(15) Balabanovich, A. I.; Luda, M. P.; Camino, G.; Hornung, A. Thermal decomposition behavior of 1,2-bis-(2,4,6-tribromophenoxy)-ethane. *J. Anal. Appl. Pyrolysis* **2003**, *67*, 95–107.

(16) Belevi, H.; Moench, H. Factors determining the element behavior in municipal solid waste incinerators. 1. Field studies. *Environ. Sci. Technol.* **2000**, *34*, 2501–2506.

(17) Huber, S.; Moe, M. K.; Schmidbauer, N.; Hansen, G. H.; Herzke, D. *Emissions from Incineration of Fluoropolymer Materials—A Literature Survey*; Norwegian Institute for Air Research: Kjeller, Norway, 2009; OR 12/2009, <http://www.nilu.no/DesktopModules/NiluWeb/UserControls/Resources/File.ashx?filename=12-2009-dhenyutgave4.pdf&filetype=file> (accessed June 6, 2014).

(18) Agency for Toxic Substances and Disease Registry (ATSDR). *Public Health Statement Fluorides*; ATSDR, Public Health Service, U.S. Department of Health and Human Services: Atlanta, GA, 2003; <http://www.atsdr.cdc.gov/toxprofiles/tp11-c1-b.pdf> (accessed June 6, 2014).

(19) Çetin, S.; Veli, S.; Ayberk, S. An investigation of halogens in Izmit hazardous and clinical waste incinerator. *Waste Manage.* **2004**, *24*, 183–191.

(20) Grabke, H. J.; Reese, E.; Spiegel, M. The effects of chlorides, hydrogen chloride, and sulfur dioxide in the oxidation of steels below deposits. *Corros. Sci.* **1995**, *37*, 1023–1043.

(21) Lehmusto, J.; Skrifvars, B. J.; Yrjas, P.; Hupa, M. Comparison of potassium chloride and potassium carbonate with respect to their tendency to cause high temperature corrosion of stainless 304L steel. *Fuel Process. Technol.* **2013**, *105*, 98–105.

- (22) Asteman, H.; Spiegel, M. Investigation of the HCl (g) attack on pre-oxidized pure Fe, Cr, Ni and commercial 304 steel at 400 °C. *Corros. Sci.* **2007**, *49*, 3626–3637.
- (23) Enestam, S.; Bankiewicz, D.; Tuiremo, J.; Mäkelä, K.; Hupa, M. Are NaCl and KCl equally corrosive on superheater materials of steam boilers? *Fuel* **2013**, *104*, 294–306.
- (24) Lehmusto, J.; Skrifvars, B. J.; Yrjas, P.; Hupa, M. High temperature oxidation of metallic chromium exposed to eight different metal chlorides. *Corros. Sci.* **2011**, *53*, 3315–3323.
- (25) Zhuang, Y.; Chen, C.; Timpe, R.; Pavlish, J. Investigations on bromine corrosion associated with mercury control technologies in coal flue gas. *Fuel* **2009**, *88*, 1692–1697.
- (26) Lai, G. Y. *High-Temperature Corrosion of Engineering Alloys*; ASM International: Materials Park, OH, 1990.
- (27) Westen-Karlsson, M. Assessment of a laboratory method for studying high temperature corrosion caused by alkali salts. Licentiate Thesis, Åbo Akademi University, Åbo, Finland, 2008.
- (28) Skrifvars, B. J.; Backman, R.; Hupa, M.; Salmenoja, K.; Valkilainen, E. Corrosion of superheater steel materials under alkali salt deposits. Part 1: The effect of salt deposit composition and temperature. *Corros. Sci.* **2008**, *50*, 1274–1282.
- (29) Bankiewicz, D.; Enestam, S.; Yrjas, P.; Hupa, M. Experimental studies of Zn and Pb induced high temperature corrosion of two commercial boiler steels. *Fuel Process. Technol.* **2013**, *105*, 89–97.
- (30) Bankiewicz, D.; Yrjas, P.; Hupa, M. High-temperature corrosion of superheater tube materials exposed to zinc salts. *Energy Fuels* **2009**, *23*, 3469–3474.
- (31) Shinata, Y. Accelerated oxidation rate of chromium induced by sodium chloride. *Oxid. Met.* **1987**, *27*, 315–332.
- (32) Ignat'eva, E. O.; Bekhtereva, E. M.; Garkushin, I. K.; Kondratyuk, I. M. Phase equilibria in the stable tetrahedron NaF–KF–KBr–K₂CrO₄ of the quaternary mutual system Na,K||F,Br,CrO₄. *Russ. J. Inorg. Chem.* **2013**, *58*, 468–473.